Laser and Particle Beams (2014), *32*, 343–351.

doi:10.1017/S0263034614000202

Experimental study of Richtmyer-Meshkov instability in a cylindrical converging shock tube

TING SI, ZHIGANG ZHAI, AND XISHENG LUO

Advanced Propulsion Laboratory, Department of Modern Mechanics, University of Science and Technology of China, Hefei, China

(RECEIVED 25 November 2013; ACCEPTED 22 April 2014)

Abstract

The interaction of a cylindrical converging shock wave with an initially perturbed gaseous interface is studied experimentally. The cylindrical converging shock is generated in an ordinary shock tube but with a specially designed test section, in which the incident planar shock wave is directly converted into a cylindrical one. Two kinds of typical initial interfaces involving gas bubble and gas cylinder are employed. A high-speed video camera combined with schlieren or planar Mie scattering photography is utilized to capture the evolution process of flow structures. The distribution of baroclinic vorticity on the interface induced by the cylindrical shock and the reflected shock from the center of convergence results in distinct phenomena. In the gas bubble case, the shock focusing and the jet formation are observed and the turbulent mixing of two fluids is promoted because of the gradually changed shock strength and complex shock structures in the converging part. In the gas cylinder case, a counter-rotating vortex pair is formed after the impact of the converging shock and its rotating direction may be changed when interacting with the reflected shock for a relatively long reflection distance. The variations of the interface displacements and structural dimensions with time are further measured. It is found that these quantities are different from those in the planar counterpart because of the shock curvature, the Mach number effect and the complex shock reflection within the converging shock tube test section. Therefore, the experiments reported here exhibit the great potential of this experimental method in study of the Richtmyer-Meshkov instability induced by converging shock waves.

Keywords: Converging shock; Gaseous interface; Richtmyer-Meshkov instability

1. INTRODUCTION

The interaction of a shock wave with an initially perturbed interface separating two fluids with different properties is generally referred to as the Richtmyer-Meshkov (RM) instability. The pioneering theoretical and numerical analysis on this shock-induced instability was performed by Richtmyer (1960) and then confirmed by Meshkov (1969) in a shock tube. From then on, a large number of theoretical, numerical, and experimental studies on the RM instability have been carried out because of its wide physical applications such as inertial confinement fusion (Lindl *et al.*, 1992), turbulent mixing in scramjet (Yang *et al.*, 1993), and collapse in supernova (Arnett *et al.*, 1989) and its great academic significance in interfacial instability, vortex dynamics, and formation of compressible turbulence. Several comprehensive reviews have been made to summarize the progress of studies on the RM instability in the past years (Zabusky, 1999; Brouillette, 2002; Ranjan *et al.*, 2011). However, most previous researches mainly focused on planar shock cases and the studies on the RM instability induced by converging shock waves are still desirable for many practical applications. Exceptional studies include numerical simulations (Mikaelian,1995; Zhang & Graham, 1998; Glimm *et al.*, 2002) and experiments (Lanier *et al.*, 2003; Hosseini & Takayama, 2005a; Fincke *et al.*, 2005), which have reported that the convergence can cause the apparent postponement of saturation and the late-time increase in growth rate. Furthermore, the converging shock can result in extreme conditions near the focal point. It is therefore significant to explore the characteristics of the RM instability with respect to converging shock cases.

Shock tube is one of the most used facilities to produce a shock wave in laboratory situations. In recent decades, attempts have been made to generate converging shock waves in shock tube environments. Perry and Kantrowitz (1951) established a horizontal annular coaxial shock tube

Address correspondence and reprint requests to: Xisheng Luo, Advanced Propulsion Laboratory, Department of Modern Mechanics, University of Science and Technology of China, Hefei, China. E-mail: xiuo@ustc.edu.cn

for the first time to observe the cylindrical converging shock. Later, Takayama *et al*. (1987) built a horizontal converging shock tube with struts supporting the inner core. Subsequently, a vertical coaxial diaphragmless shock tube was constructed to produce uniform cylindrical converging shock waves (Hosseini *et al*., 2000). Cylindrical converging shock wave was also generated in a shock tube with a shock-shaping end section (Apazidis & Lesser, 1996; Apazidis *et al*., 2002; Kjellander *et al*., 2011). Besides, Dimotakis and Samtaney (2005) reported a gas lens technique in a two-dimensional wedge geometry and Hosseini and Takayama (2005b) designed an aspheric lens-shaped transparent test section to produce converging shock waves. It must be mentioned that so far the RM instability experiments have seldom been performed in such shock tubes probably due to the difficulties in settling the initial interfaces and measuring relevant quantities. Recently, a simple but effective technique for generating cylindrical converging shock waves in an ordinary shock tube was developed based on shock dynamics theory in our group (Zhai *et al*., 2010; Luo *et al*., 2014). The present experimental study is motivated by the method, aiming at more potential of this experimental method in study of the RM instability.

In experimental aspect of the RM instability study, the generation of initially perturbed interface and the employment of diagnostic methods are very important. Interfaces used in previous experiments can mainly be classified into two types, i.e., with and without membranes. Interfaces with membrane consist of soap film interface (Haas & Sturtevant, 1987; Ranjan *et al*., 2005; Layes *et al*., 2009; Zhai *et al*., 2011; Si *et al*., 2012; Wang *et al*., 2013; Luo *et al*., 2013) and microfilm interface (Bates & Nikiforakisb, 2007; Mariani *et al*., 2008). In these methods, the shape of interface with sharp boundaries can accurately be determined. The other type of interface is considered to be membraneless interface, which includes gas cylinders (Jacobs, 1993; Tomkins *et al*., 2008; Zou *et al*., 2010), gas curtains (Jacobs *et al*., 1992; Orlicz *et al*., 2009; Balasubramanian *et al*., 2012), single-mode interfaces by vibration (Sheeley & Jcobs, 1995; Jones & Jacobs, 1997; Jacobs & Krivets, 2005; Long *et al*., 2009), interfaces by retracting metal plate initially separating two different gases (Puranik *et al*., 2004) and some others. In these methods, the influences of membrane and support would be avoided, but gaseous diffusion often happens initially between two fluids and the exact initial conditions have to be determined afterward. From the above-mentioned methods, different shapes of gaseous interface can be obtained, including single and multi-mode interfaces (Mariani *et al*., 2008; Long *et al*., 2009; Balasubramanian *et al*., 2012), spherical bubbles (Ranjan *et al*., 2011), circular cylinders (Hass & Sturtevant, 1987; Hosseini & Takayama, 2005a; Tomkins *et al*., 2008), elliptical cylinders (Zou *et al*., 2010), and polygonal blocks (Bates & Nikiforakisb, 2007; Wang *et al*., 2013). As to the diagnostics, various methods such as shadowgraphy (Hass & Sturtevant, 1987; Layes *et al*., 2009), schlieren (Zhai *et al*., 2011), double-exposure holographic interferometry (Hosseini & Takayama, 2005a), and laser sheet imaging (Brouillette, 2002; Ranjan *et al*., 2011; Orlicz *et al*., 2013) have been used. As a result, rich phenomena and relevant quantities of the distorted interface can be obtained for understanding the physical rules and mechanisms of the RM instability.

When a shock wave passes through an initially perturbed interface, baroclinic vorticity will be generated due to the misalignment between the density and pressure gradients. The development behaviors of gaseous interfaces are closely dependent on the amplitude and distribution of baroclinic vorticity, which is attributed to the shock strength and the initial shapes of both interface and shock wave. In our previous study (Si *et al*., 2014), some preliminary experiments were performed based on the interaction of a cylindrical shock with a heavy-gas cylinder and it was found that the results are different from ones with respect to the planar shock. In this work, we will revisit two types of interface used in planar shock cases, i.e., gas bubble and gas cylinder, and settle them in the cylindrical converging shock tube to investigate the evolution of such interfaces accelerated by the converging shock and the reflected shock formed from the center of convergence.

2. EXPERIMENTAL METHODS

2.1. Generation of Cylindrical Shock Waves

Here we will restrict ourselves to the RM instability experiments and briefly describe the generation of cylindrical shock waves. For the detailed mathematical formulism and validation, the reader is referred to our previous work (Zhai *et al*., 2010; 2012; Luo *et al*., 2014). Figure 1 illustrates the schematic of the test section which can directly convert an incident planar shock wave into a cylindrical one. The test section mainly consists of a straight wall (OAA′O′) and a curved wall (OBB′O′) designed based on the shock dynamics theory (Zhai *et al*., 2010). The wall profile (curved line from point B (B′) to point Q (Q′)) can be obtained for a given group of controllable parameters including the converging angle θ_0, the incident planar shock Mach number M_0 and the shock tube height h. In order to optimize the experimental observation and measurement, a sufficient

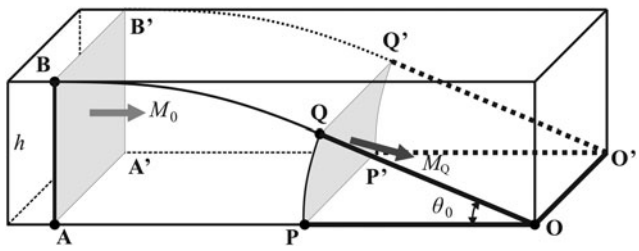

Fig. 1. Schematic of the test section. M_0, the incident planar shock Mach number; θ_0, the converging angle; j, the shock tube height; M_q, the Mach number at point Q.

https://doi.org/10.1017/S0263034614000202 Published online by Cambridge University Press

converging part (OPQ-O′P′Q′) is needed. Generally, large M_0, large h, and moderate θ_0 will be favorable for performing RM instability experiments (Zhai *et al*., 2012).

Experiments are conducted in two sets of horizontal rectangular shock tubes with different h, respectively. The first shock tube (ST-1) consists of a 1.7 m driver section and a 2.5 m driven section with cross-sectional area of 70 mm × 40 mm (i.e., $h = 70$ mm or 40 mm), and the second shock tube (ST-2) consists of a 2.0 m driver section and a 7.0 m driven section with cross-sectional area of 95 mm × 95 mm (i.e., $h = 95$ mm). For each shock tube, the controllable parameters M_0, h, and θ_0 are chosen to calculate the wall profile and the test section is then manufactured accurately by the linear cutting technique. Initially, both the driver and driven sections of the ST-1 or ST-2 are full of air at atmospheric pressure and the driver section is further filled with nitrogen to generate the incident planar shock by the rupture of a polypropylene diaphragm initially separating two sections. The velocity (or the Mach number) of the incident shock is determined by the signals of two piezoelectric pressure transducers mounted on the shock tube side wall.

2.2. Formation of Initial Interfaces

The experimental facility is capable of settling most abovementioned interfaces with arbitrary shapes. In this work, we mainly focus on spherical and cylindrical gaseous interfaces making use of heavy tested gas (i.e., SF_6), as sketched in Figure 2. Soap film is used to create the spherical gaseous interface. Soap film component is very thin (about 0.25–1 μm), flimsy, and durable so that its presence may have very little influence on experiments. The spherical gaseous interface is formed by filling a soap bubble with SF_6 and the bubble is hung on a top support in the test section. The gas cylinder flowing vertically under gravity into the test section is created in a careful procedure similar to previous studies (Tomkins *et al*., 2008; Si *et al*., 2014). Prior to experiments glycol droplets produced by a commercial theatrical fog generator are well mixed with the tested gas and served as tracer. The accurate track of glycol droplets in SF_6 has been confirmed by Prestridge *et al*., (2000). The heavy gas cylinder flows slowly (~0.1 m/s) through a round nozzle on the top wall and is sucked mildly through a plenum on the bottom wall by a vacuum pump. In this way the gas cylinder moves steadily with smooth edges.

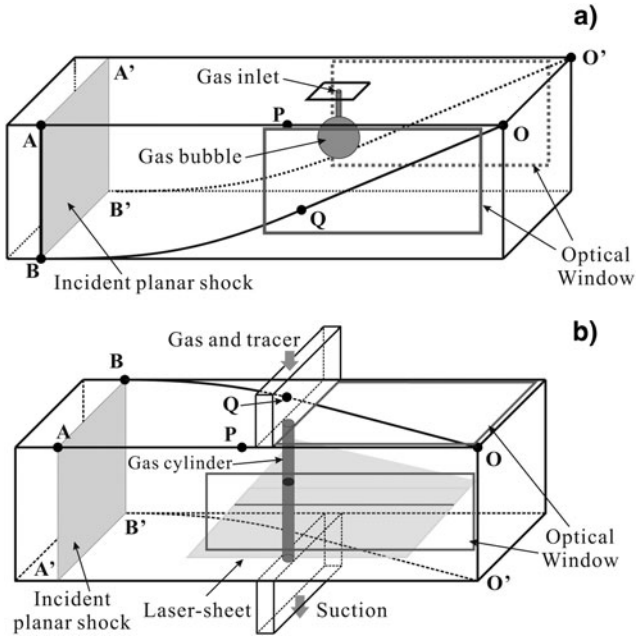

Fig. 2. Schematics of experimental setup corresponding to (**a**) gas bubble and (**b**) gas cylinder.

2.3. Flow Diagnostics

A high-speed video camera (FASTCAM SA5, Photron Limited) is utilized to record the evolution of interfaces based on two optical systems. Figure 3 presents the schematics of the shock tube and flow diagnostic system. The first one is the schlieren photography as shown in Figure 3a, in which a Z-fold schlieren system made up of a knife-edge, a slit, two convex lenses, and two concave mirrors is adopted and the flow field is illuminated by a DC regulated light source (DCR III, SCHOTT North America, Inc., 200 W). Another optical system is the planar Mie scattering photography as sketched in Figure 3b, in which a laser-sheet illuminating the flow is provided by a continuous laser (SDL-532-15000T, Shanghai Dream Lasers technology Co. Ltd., 15 W, 532 nm) combined with a cylindrical concave mirror and a convex lens. An inclined flat mirror located in front of the test section is used to easily adjust the position of the laser-sheet and make sure that the laser-sheet is perpendicular to the axis of gas cylinder (see Fig. 2b). The timing and triggering system involves a four channel delay generator (DG645, Stanford Research Systems), two piezoelectric pressure transducers, a charge amplifier, an oscilloscope, and some accessories. The schlieren photography records the shock propagation and interface deformation in an integrated view, while the planar Mie scattering photography monitors the flow based on the additional tracer in a cross-sectional view. Depending on the initial conditions in experiments, different optical systems are employed.

3. RESULTS AND DISCUSSION

3.1. Gas Bubble

The shock-bubble interaction is a fundamental configuration for studying the RM instability and the planar shock case has been well understood (Ranjan *et al*., 2011). In this work, the experiment is conducted in the ST-1 with chosen parameters $M_0 = 1.2$, $\theta_0 = 15°$ and $h = 70$ mm. The initial Mach number at point Q and the radius of the converging part are calculated from the shock dynamics theory as $M_q = 1.29$ and $R_q = 106$ mm, respectively. The bubble diameter $D_0 = 16$ mm and the distance from the bubble center to the

https://doi.org/10.1017/S0263034614000202 Published online by Cambridge University Press

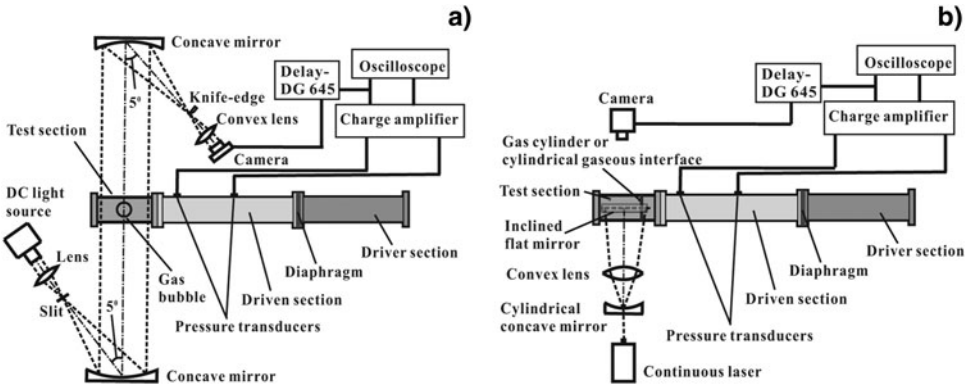

Fig. 3. Schematics of the shock tube and flow diagnostics including (**a**) the schlieren system (the parallel light passes through the test section and the flow is recorded in an integrated view) and (**b**) the planar Mie scattering system (the laser-sheet is perpendicular to the interface axis and the flow is recorded in a cross-sectional view).

center of convergence $L_0 = 86$ mm are measured, respectively. A pair of optical windows of 70 mm × 150 mm are located at the position where the converging part is in sight, as shown in Figure 2b. The flow is monitored by the high-speed schlieren photography, as indicated in Figure 3a. The high-speed video camera with a frame rate of 50,000 fps corresponding to the time interval between two consecutive frames of 20 μs, a spatial resolution of 192 × 704 and a very fast shutter of down to 1 μs is adopted.

The evolution process of the shock propagation and the bubble deformation is captured in a single test run as presented in Figure 4. At the beginning the incident shock moves into the converging part and the shock front bends to a circular arc (frame 0). When the cylindrical shock passes across the SF_6 bubble, a reflected shock moves back and a refracted shock propagates inside the gas volume more slowly than the incident shock due to the larger acoustic impedance inside the bubble (frames 1 to 3). Then typical phenomena including the shock focusing and the jet formation appear (frame 4). In this process the refracted shock converges to a very small zone inside the SF_6 bubble, resulting in very high pressure that promotes the interface deformation. As time proceeds, the SF_6 jet is elongated and the interface body develops into a vortex ring (frames 5 to 9). Later on, as the shock reflects from the center of convergence and interacts with the evolving interface (frames 14 to 22), the evolution of the interface is intensified and the flow quickly resembles turbulent mixing.

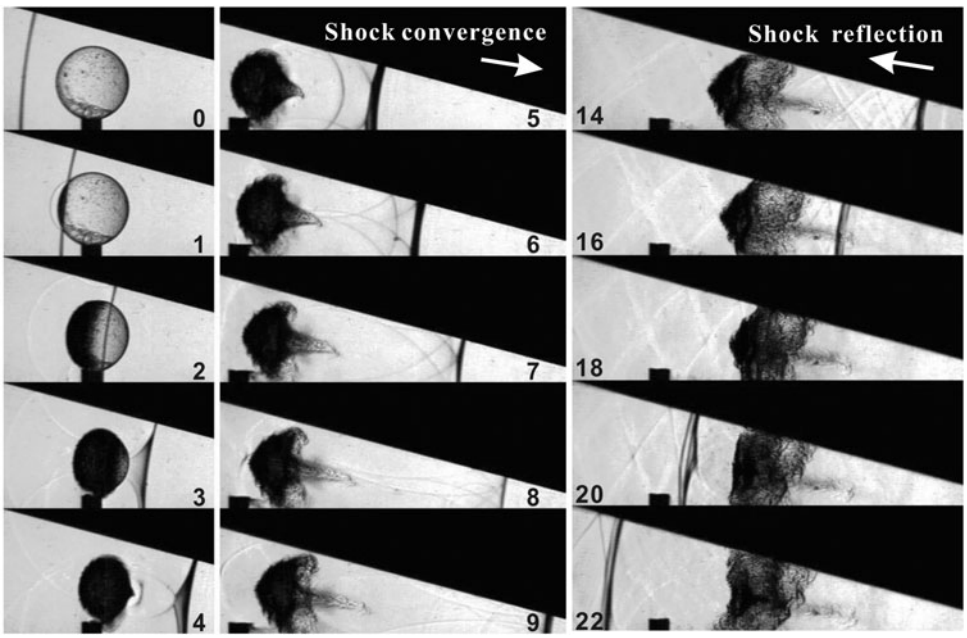

Fig. 4. Sequence of schlieren frames showing the evolution of the SF_6 bubble with frame rate of 50,000 fps corresponding to a time interval between two consecutive frames of 20 μs.

https://doi.org/10.1017/S0263034614000202 Published online by Cambridge University Press

Note that the phenomenon presented here is similar to that in the planar shock case (Zhai *et al*., 2011; Si *et al*., 2012), but a great difference between them exists. On one hand, the shock focusing coming from the cylindrical shock acceleration is much stronger because of the gradually enhanced shock strength, thus the SF_6 jet moves more quickly for the same incident shock strength. On the other hand, the shock structure seems more complex in the converging situation. For example, the transmitted and refracted shock waves propagating toward the center of convergence impinge on the wedge walls and the reflected waves will impact with the distorted interface again. These additional waves will certainly complicate the interaction process.

The displacements and structural scales of the interface are further measured. Figure 5 gives the variations of the interface displacements for the left and the right interfaces (assuming the incident shock moves from left to right as inserted in the figure) and structural dimensions including the interface length and the vortex ring length. The positions of measurement always refer to the leftmost or rightmost portion of the interface. At the beginning, the left interface first obtains a velocity while the right interface is still stationary. Then the left interface keeps moving with nearly the same velocity and the right interface moves quickly because of the SF_6 jet formation. In this stage, the velocities of the left and right interfaces are estimated to be about 67.7 m/s and 156.6 m/s, respectively. As the reflected shock arrives and interacts with the evolving interface, the SF_6 jet is first compressed, obtains a sudden opposite velocity, and finally diffuses gradually. In the process, the left interface first stops moving and then moves back with a very small velocity (about 8.8 m/s). Due to the variation of the interface displacements, the structural dimensions of the interface also change with time, as shown in Figure 5b. After the incident shock passage, the interface length decreases because of the compression. As the SF_6 jet and the vortex ring are formed, all interface structures increase in size. When the reflected shock arrives, the interface length and the vortex ring length start decreasing. At the late stage the intensified mixing between two fluids makes the overall length increase.

3.2. Gas Cylinder

The gas cylinder is one of the typical membraneless interfaces widely used in past RM instability experiments with respect to a planar shock wave (Jacobs, 1993; Tomkins *et al*., 2008). In this work, the shock tube (ST-2) with $M_0 = 1.2$, $\theta_0 = 15°$, and $h = 95$ mm which are obtained theoretically (Si *et al*., 2014) is used. The SF_6 cylinder well mixed with glycol droplets is positioned within the converging part. The diameter D_0 of the gas cylinder and the distance L_0 from the gas cylinder axis to the center of convergence can be adjusted. It should be pointed out that besides the feature of the gas cylinder (e.g., D_0 and L_0), the initial conditions in experiments cover the shape of the test section (e.g., M_0, θ_0, and h) and the category of the gas (e.g., SF_6, krypton, argon, and others). In present work, we mainly focus on the influence of L_0 and more studies are the scope of our next work. Here the diameter $D_0 = 5$ mm and two different distances ($L_0 =$ 93.3 mm and $L_0 = 115.5$ mm) are adopted. The flow is monitored by the continuous laser-sheet imaging method, as sketched in Figure 3b. Different frame rates of the high-speed video camera (30,000 fps and 35,000 fps) are used for different temporal and spatial resolutions (the corresponding time intervals are 33.3 μs and 28.6 μs and spatial resolutions are 256×800 and 192×856, respectively). The shutter of the camera is down to 1 μs. The width of the laser-sheet is carefully adjusted in order to gain an acceptable scattering light intensity when the flow field is illuminated.

Figures 6 and 7 present the sequences of cross-sectional view of the SF_6 cylinder accelerated by the cylindrical converging shock and the reflected shock from the center of convergence (assuming the incident shock moves from bottom to top as shown in the figure). Note that the initial conditions have been confirmed by the direct observation of the flow prior to each run. For $L_0 = 93.3$ mm, the shock Mach number is about 1.35 when the cylindrical shock impacts with the SF_6 cylinder. At the beginning, the SF_6 cylinder

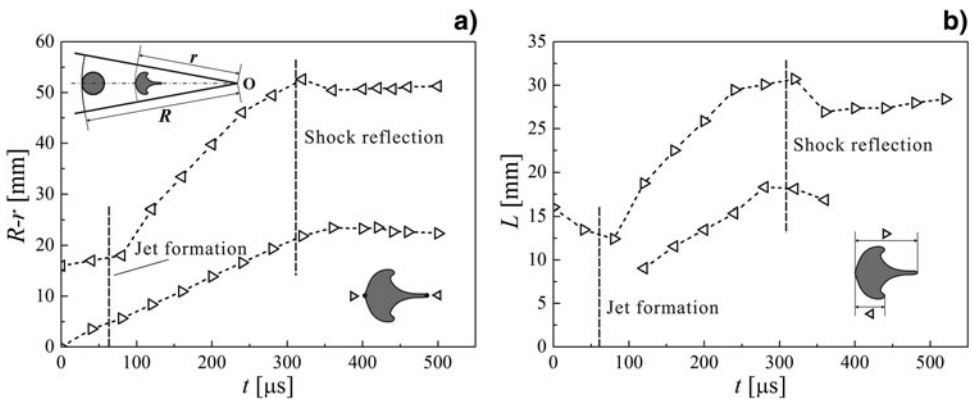

Fig. 5. Variations of the gas bubble development: (**a**) displacements and (**b**) dimensions of the interface structures.

https://doi.org/10.1017/S0263034614000202 Published online by Cambridge University Press

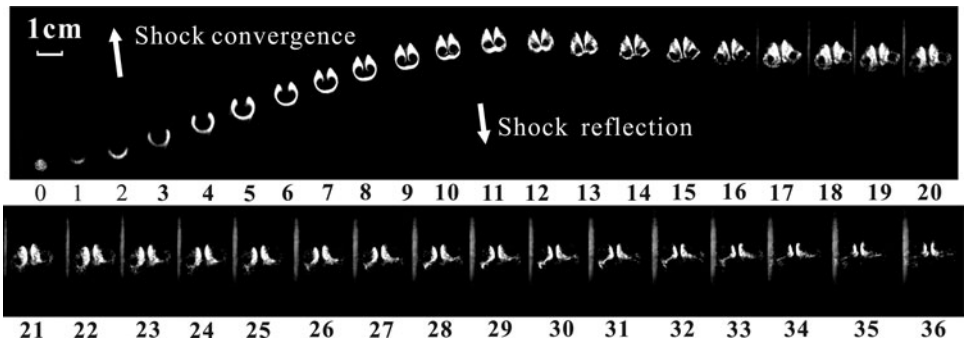

Fig. 6. Sequence of laser-sheet frames showing the cross-sectional view of the SF_6 cylinder for $L_0 = 93.3$ mm with frame rate of 30,000 fps (the corresponding time interval is 33.3 μs).

develops into a crescent shape quickly. As time proceeds, a counter-rotating vortex pair is formed due to the baroclinic vorticity initially deposited on the boundary of the gas cylinder. As the evolving interface undergoes the reflected shock, the vortex pair gathers most of the interface mass at its top boundaries and continues rotating in the same directions. The bottom arcuate interface becomes flat and then breaks up into two parts, moving together with the vortex pair. At late times, the vortex pair diffuses gradually due to the mixing of two gases. For $L_0 = 115.5$ mm, the shock Mach number is about 1.32 when the cylindrical shock arrives at the position of the SF_6 cylinder. In the early stage, the evolution of the interface is similar to that described above. As the reflected shock arrives, the evolving interface suddenly stops moving onward and the top vortex pair rolls up with opposite rotating directions. Later on, the bottom circular interface grows in size and gradually diffuses, and the top vortex pair enhances the mixing of the SF_6 gas with the ambient air.

It is interesting that there is a reversal of the rotating direction of the re-accelerated vortex pair when the value of L_0 increases. The previous experimental results for $L_0 =$ 181.5 mm (Si *et al.*, 2014) also demonstrated this observation. The differences between these cases are mainly attributed to the Mach number effect, or rather, to the generation and distribution of baroclinic vorticity due to the misalignment between the density and pressure gradients. On one hand, the initial shock Mach numbers are different when the cylindrical shock impacts with the SF_6 cylinder for different L_0. A larger L_0 corresponds to a smaller initial shock Mach number. On the other hand, although the initial gas cylinder diameter and the cylindrical shock shape are nearly the same for these cases, the evolving interfaces between them at the time when the reflected shock arrives are different due to the different time period of evolution. As a whole, the rotating direction of the vortex pair is dependent on the positive and negative values of the superposed baroclinic vorticity deposited on the interface.

Figure 8 presents the experimental data for both $L_0 =$ 93.3 mm and $L_0 = 115.5$ mm showing the variation with time of the interface displacements for the left and the right interfaces (assuming the incident shock moves from left to right as inserted in the figure) and structural dimensions including the interface length and the vortex pair core distance. Before the arrival of the reflected shock, both the left and the

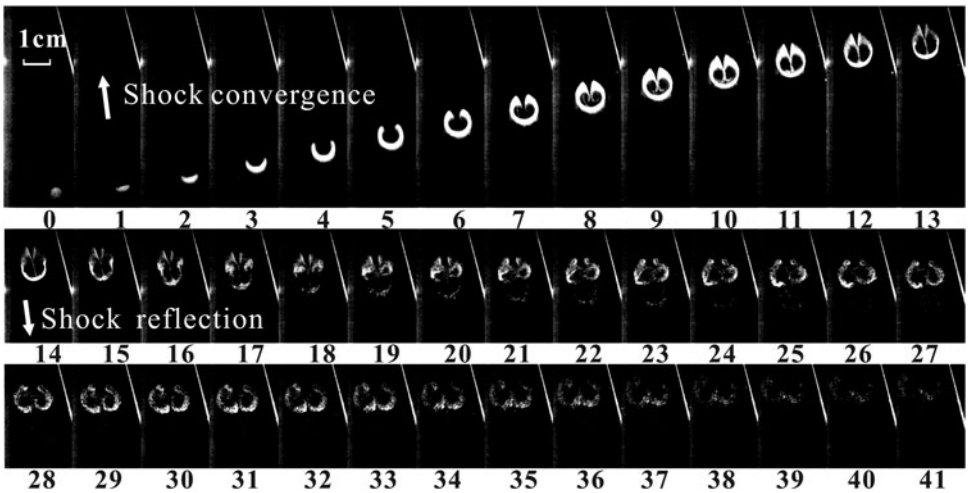

Fig. 7. Sequence of laser-sheet frames showing the cross-sectional view of the SF_6 cylinder for $L_0 = 115.5$ mm with frame rate of 35,000 fps (the corresponding time interval is about 28.6 μs).

https://doi.org/10.1017/S0263034614000202 Published online by Cambridge University Press

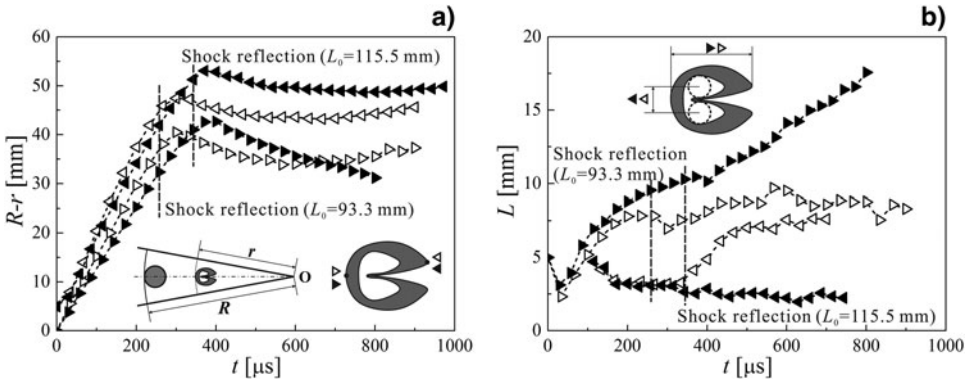

Fig. 8. Variations of the gas cylinder development: (**a**) displacements and (**b**) dimensions of the interface structures. Solid symbol: L_0 = 115.5 mm; hollow symbol: L_0 = 93.3 mm.

right interfaces move toward the center of convergence and the velocities of the interface for L_0 = 93.3 mm are larger than those for L_0= 115.5 mm. The difference mainly comes from their different shock Mach numbers as the cylindrical shock wave interacts with the SF_6 cylinder. In this period, the right interface moves more quickly than the left interface due to the development of the vortex pair. When the reflected shock propagates through the evolving bubble, each interface suddenly stops moving and then obtains a negative velocity. Although the rotating directions of the main vortex pair are opposite for L_0 = 93.3 mm and L_0 = 115.5 mm, the tendencies of the interface structures changing with time between them have the similar regularity except when the evolving interface for L_0 = 115.5 mm develops into a reversed vortex pair and a circular interface at the late stage. The overall lengths of the interfaces for both L_0 = 93.3 mm and L_0 = 115.5 mm are plotted in Figure 8b, where the vortex pair core distance is also given. Before the arrival of the reflected shock, the interface length first decreases because of the incident shock passage and then gradually increases after the generation of the vortex pair. In this process, the transmitted and refracted shock waves propagating toward the center of convergence reflect from the wedge walls and further compress the interface, making the vortex pair core distance be reduced. After the reflected shock passes through the distorted interface, different phenomena for L_0 = 93.3 mm and L_0 = 115.5 mm result in different tendencies of the structural dimensions changing with time. For L_0 = 93.3 mm, as the counter-rotating vortex pair develops still in the same direction, the overall interface length first decreases in a very short time period and then slightly increases, and the vortex pair core distance first keeps nearly constant and then gradually increases. Later on, both of the structural scales seldom change accompanied with the diffusion of the interface. For L_0 = 115.5 mm, the overall interface length always increases in the process except when the reflected shock just impacts with the evolving interface, and the vortex pair core distance seems decreasing all the time. One can find oscillations appearing within the experimental data, which may be caused by the interaction of the interface with the shock reflected from the wedge walls of the shock tube test section. As a whole, the complete process of the interface evolution can be revealed by the variations of the interface structures with time.

4. CONCLUSIONS

Experiments have been carried out to explore the potential of experimental method in study of RM instability induced by cylindrical converging shock waves. The test section of the shock tube was well designed based on shock dynamics theory to directly convert the incident planar shock into the cylindrical one. Spherical and cylindrical gaseous interfaces were employed in two sets of shock tubes with different control parameters. High-speed imaging combined alternately with two optical systems including schlieren and planar Mie scattering photography was utilized to capture the evolution of flow structures in a single test run for each case. Rich phenomena have been observed in different cases. The typical shock focusing and jet formation are found corresponding to the gas bubble. The counter-rotating vortex pair is formed in case of gas cylinder and a reversal is obtained when the position of the gas cylinder in the test section changes. The experiments also indicate that the phenomena of the interface accelerated by the converging shock and the reflected shock formed from the center of convergence are a little similar to those found in the planar shock cases, but differences also exist between them because of the shock curvature and Mach number effects in the converging cases, which can be attributed to the baroclinic mechanism due to the misalignment of density and pressure gradients. The experimental facility reported here provides a significant tool in study of RM instability with respectto converging shock waves. It must be mentioned that more experimental results and quantitative analysis are planned to be performed in the future. The effects of initial conditions on the growth rate of perturbations and the turbulent mixing of two gases should be studied thoroughly in order to go deep into the physical mechanism of interface evolution and compressible turbulence.

https://doi.org/10.1017/S0263034614000202 Published online by Cambridge University Press

ACKNOWLEDGMENTS

The authors would like to thank Xiansheng Wang and Fu Zhang for their help during the experiments. The work was supported by the National Natural Science Foundation of China (11272308 and 11302219), the Knowledge Innovation Program of the Chinese Academy of Sciences (GY2011053006), and the Fundamental Research Funds for Central Universities (WK2090050020).

REFERENCES

Apazidis, N. & Lesser, M. B. (1996). On generation and convergence of polygonal-waves. *J. Fluid mech.* **309**, 301–319.

Apazidis, N., Lesser, M. B., Tillmark, N. & Johansson, B. (2002). An experimental study of converging polygonal shock waves. *Shock Waves* **12**, 39–58.

Arnett, W. D., Bahcall, J. N., Kirshner, R. P. & Woosley, S. E. (1989). Supernova 1987a. *Annu. Rev. Astron. Astrophys.* **27**, 629–700.

Balasubramanian, S., Orlicz, G. C., Balakumar, B. J. C. & Prestridge, K. P. (2012). Experimental study of initial condition dependence on Richtmyer-Meshkov instability in the presence of reshock. *Phys. Fluids* **24**, 031403.

Bates, K. R. & Nikiforakisb, N. (2007). Richtmyer-MeShkov instability induced by the interaction of a shock wave with a rectangular block of SF6. *Phys. Fluids* **19**, 036101.

Brouillette, M. (2002). Richtmyer-Meshkov instability. *Annu. Rev. Fluid Meeh.* **34**, 445–468.

Dimotakis, P. E. & Samtaney, R. (2005). Planar shock cylindrical focusing by a perfect-gas lens. *Phys. Fluids* **18**, 031705.

Fincke, J. R., Lanier, N. E., Batha, S. H., Hueckstaedt, R. M., Magelssen, G. R., Rothman, S. D., Parker, K. W. & Horsfield, C. J. (2005). Effect of convergence on growth of the Richtmyer-Meshkov instability. *Laser Part. Beams* **23**, 2125.

Glimm, J., Grove, J., Zhang, Y. & Dutta, S. (2002). Numerical study of axisymmetric Richtmyer-Meshkov instability and azimuthal effect on spherical mixing. *J. Stat. Phys.* **107**, 241–260.

Haas, J. F. & Sturtevant, B. (1987). Interaction of weak shock waves with cylindrical and spherical gas inhomogeneities. *J. Fluid Meeh.* **181**, 41–76.

Hosseini, S. H. R., Onodera, O. & Takayama, K. (2000). Characteristics of an annular vertical diaphragm less shock tube. *Shock Waves* **10**, 151–158.

Hosseini, S. H. R. & Takayama, K. (2005*a*). Experimental study of Richtmyer-Meshkov instability induced by cylindrical shock waves. *Phys. Fluids* **17**, 084101.

Hosseini, S. H. R. & Takayama, K. (2005*b*). Implosion of a spherical shock wave reflected from a spherical wall. *J. Fluid Meeh.* **530**, 223–239.

Jacobs, J. W. (1993). The dynamics of shock accelerated light and heavy gas cylinders. *Phys. Fluids A* **5**, 2239–2247.

Jacobs, J. W., Klein, D. L., Jenkins, D. G. & Benjamin, R. F. (1992). Instability growth patterns of a shock-accelerated thin fluid layer. *Phys. Rev. Lett.* **70**, 583–589.

Jacobs, J. W. & Krivets, V. V. (2005). Experiments on the late-time development of single mode Richtmyer-Meshkov instability. *Phys. Fluids* **17**, 034105.

Jones, M. A. & Jacobs, J. W. (1997). A membraneless experiment for the study of Richtmyer-Meshkov instability of a shock-accelerated gas interface. *Phys. Fluids* **9**, 3078–3085.

Kjellander, M., Tillmark, N. & Apazidis, N. (2011). Experimental determination of selfsimilarity constant for converging cylindrical shocks. *Phys. Fluids* **23**, 0116103.

Lanier, N. E., Barnes, C. W., Batha, S. H., Dar, R. D., Magelssen, G. R., Scott, J. M., Dunne, A. M., Parker, K. W. & Rothman, S. D. (2003). Multimode seeded RichtmyerMeshkov mixing in a convergent, compressible, miscible plasma system. *Phys. Plas.* **10**, 1816–1821.

Layes, G., Jourdan, G. & Houas, L. (2009). Experimental study on a planeshock wave accelerating a gas bubble. *Phys. Fluids* **21**, 074102.

Lindl, J. D., Mccrory, R. L. & Campbell, E. M. (1992). Progress toward ignition and burn propagation in inertial confinement fusion. *Phys. Today.* **45**, 32–40.

Long, C. C., Krivets, V. V., Greenough, J. A. & Jacobs, J. W. (2009). Shock tube experiments and numerical simulation of the single-mode, three-dimensional Richtmyer-Meshkov instability. *Phys. Fluids* **21**, 114104.

Luo, X., Si, T., Yang, J. & Zhai, Z. (2014). A Cylindrical converging shock tube for shock interface studies. *Rev. Sci. Instrum.* **85**, 015107.

Luo, X., Wang, X. & Si, T. (2013). The Richtmyer-Meshkov instability of a three-dimensional air/SF6 interface with a minimum-surface feature. *J. Fluid Mech.* **722**, 1–11.

Mariani, C., Vandenboomgaerde, M., Jourdan, G., Souffland, D. & Houas, L. (2008). Investigation of the Richtmyer-Meshkov instability with stereolithographed interfaces. *Phys. Rev. Lett.* **100**, 254503.

Meshkov, E. E. (1969). Instability of the interface of two gases accelerated by a shock wave. *Fluid Dyn.* **4**, 101–104.

Mikaelian, K. O. (1995). RayleighTaylor and RichtmyerMeshkov instabilities in finite-thickness fluid layers. *Phys. Fluids* **7**, 888890.

Orlicz, G. C., Balakumar, B. J. C. & Prestridge, K. P. (2013). Incident shock Mach number effects on Richtmyer-Meshkov mixing in a heavy gas layer. *Phys. Fluids* **25**, 114101

Orlicz, G. C., Balakumar, B. J. C., Tomkins, C. D. & Prestridge, K. P (2009). A mach number study of the Richtmyer-Meshkov instability in a varicose, heavy-gas curtain. *Phys. Fluids* **21**, 064102.

Perry, R. W. & Kantrowitz, A. (1951). The production and stability of converging shock waves. *J. Appl. Phys.* **22**, 878–886.

Prestridge, K. P., Rightley, P. M., Vorobieff, P., Benjamin, R. F. & Kurnit, N. A. (2000). Simultaneous density-field visualization and PIV of a shock-accelerated gas curtain. *Exp. Fluids* **29**, 339–346.

Puranik, P. B., Oakley, J. G., Anderson, M. H. & Bonazza, R. (2004). Experimental study of the Richtmyer-Meshkov instability induced by a Mach 3 shock wave. *Shock Waves* **13**, 413–429.

Ranjan, D., Anderson, M., Oakley, J. & Bonazza, R. (2005). Experimental investigation of a strongly shocked gas bubble. *Phys. Rev. Lett.* **94**, 184507.

Ranjan, D., Oakley, J. & Bonazza, R. (2011). Shock-bubble interactions. *Annu. Rev. Fluid Meeh.* **43**, 117–140.

Richtmyer, R. D. (1960). Taylor instability in shock acceleration of compressible fluids. *Commun. Pure Appl. Math.* **13**, 297–319.

Sheeley, J. M. & Jacobs, J. W. (1995). Experimental study of incompressible Richtrnyer- Meshkov instability. *Phys. Fluids* **8**, 405–415.

Si, T., Zhai, Z., Luo, X. & Yang, J. (2012). Experimental studies of reshocked spherical gas interfaces. *Phys. Fluids* **24**, 054101.

Si, T., Zhai, Z., Luo, X. & Yang, J. (2014). Experimental study on a heavy-gas cylinder accelerated by cylindrical converging shock waves. *Shoek Waves* **24**, 3–9.

Takayama, K., Kleine, H. & Gronig, H. (1987). An experimental investigation of the stability of converging cylindrical shock waves in air. *Exps. Fluids* **5**, 315–322.

Tomkins, C. D., Kumar, S., Orlicz, G. C. & Prestridge, K. P. (2008). An experimental investigation of mixing mechanisms in shock-accelerated flow. *J. Fluid Mech.* **611**, 131–150.

Wang, M., Si, T. & Luo, X. (2013). Generation of polygonal gas interfaces by soap film for Richtrnyer-Meshkov instability. *Exp. Fluids* **54**, 1427.

Yang, J., Kubota, T. & Zukoski, E. E. (1993). Applications of shock-induced mixing to supersonic combustion. *AIAA J.* **35**, 854–862.

Zabusky, N. (1999). Vortex paradigm for accelerated inhomogeneous flows: visiometrics for the Rayleigh-Taylor and Richtmyer-Meshkov environments. *Annu. Rev. Fluid Meeh.* **31**, 495–536.

Zhai, Z., Liu, C., Qin, F., Yang, J. & Luo, X. (2010). Generation of cylindrical converging shock waves based on shock dynamics theory. *Phys. Fluids* **22**, 041701.

Zhai, Z., Si, T., Luo, X. & Yang, J. (2011). On the evolution of spherical gas interfaces accelerated by a planar shock wave. *Phys. Fluids* **23**, 084104.

Zhai, Z., Si, T., Luo, X., Yang, J., Liu, C., Tan, D. & Zou, L. (2012). Parametric study of cylindrical converging shock waves generated based on shock dynamics theory. *Phys. Fluids* **24**, 026101.

Zhang, Q. & Graham, M. J. (1998). A numerical study of RichtmyerMeshkov instability driven by cylindrical shocks. *Phys. Fluids* **10**, 974–992.

Zou, L., Liu, C., Tan, D., Huang, W. & Luo, X. (2010). On interaction of shock wave with elliptic gas cylinder. *J. Visual.* **13**, 347–353.

https://doi.org/10.1017/S0263034614000202 Published online by Cambridge University Press